Available online at www.sciencedirect.com
SCIENCE DIRECT®
Journal of Sound and Vibration 280 (2005) 211–234
JOURNAL OF SOUND AND VIBRATION
www.elsevier.com/locate/jsvi

Dynamic modelling of a shape memory alloy adaptive tuned vibration absorber

K.A. Williams[a,*], G.T.-C. Chiu[b], R.J. Bernhard[b]

[a] *Department of Mechanical Engineering, The University of Alabama, 164 Hardaway Hall, Box 870276, Tuscaloosa, AL 35487-0276, USA*

[b] *1077 Herrick Laboratories, Purdue University, West Lafayette, IN 47907-1077, USA*

Received 2 December 2002; accepted 4 December 2003

Abstract

Shape memory alloy (SMA) adaptive tuned vibration absorbers show great potential for adaptive–passive vibration control. Heating the SMA spring element in an ATVA changes the SMA elastic modulus, which results in changing the device natural frequency. With proper design, SMA ATVA may be tuned to attenuate harmonic vibration of a primary system for a range of frequencies. Continuous tuning of the SMA ATVA is realized through modulating the temperature of the SMA spring elements. A perceived limitation of SMA in vibration control applications has been a potentially large temperature hysteresis accompanying the martensitic transformation in SMA. However, with appropriate heat treatment, a rhombohedral phase (R-phase) transformation may be achieved in the material without significant hysteresis. This paper discusses the development and modelling of a continuously tuned SMA ATVA utilizing an R-phase transformation to realize online variation of the ATVA natural frequency. The models are developed for use in feedback control of an SMA ATVA. An appropriate control goal for such controllers is defined and verified.

1. Introduction

Forced harmonic vibration is a common problem in machinery. The undesirable effects of harmonic vibration range from human discomfort to machinery failure due to fatigue and accelerated wear. A great deal of research has been done to address the control of harmonic vibration. Solutions include structural redesign, addition of passive or active vibration control devices, and, more recently, application of adaptive–passive devices. The tuned vibration absorber

*Corresponding author. Tel.: 1-205-348-2605; fax: 1-205-348-6419.
E-mail address: kwilliams@coe.eng.ua.edu (K.A. Williams).

0022-460X/$ - see front matter © 2004 Elsevier Ltd. All rights reserved.
doi:10.1016/j.jsv.2003.12.040

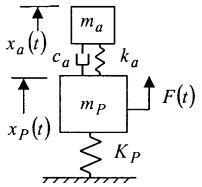

Fig. 1. TMD/TVA applied to a primary system.

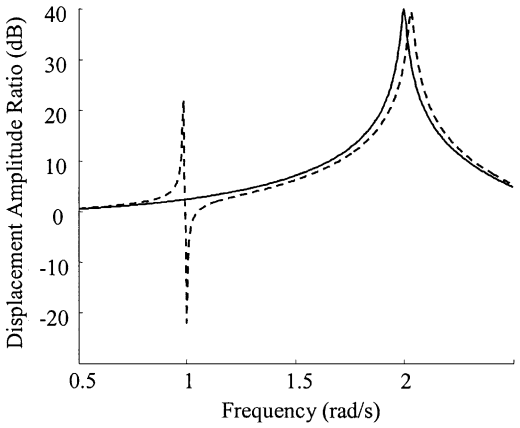

Fig. 2. Frequency response of a primary system: —, without TVA; - -, with TVA.

(TVA) shown in Fig. 1 is a classical example of a passive vibration control device. A TVA is typically lightly damped and has a natural frequency ω_a tuned to match the excitation frequency ω_{exc}, with resulting significant attenuation in the vibration of the primary system as shown in Fig. 2. However, due to the introduction of the nearby second resonance peak, as shown in Fig. 2, TVA usage is not generally desirable for situations where ω_{exc} is unknown or varies,.

The tuned mass damper (TMD) is conceptually similar to a TVA. However, in a TMD, damping is used to achieve wideband minimization of a primary system's vibration amplitude. The TMD is better suited for transient or random vibration than the TVA, but cannot, in general, achieve the performance of a TVA for steady state harmonic vibration. Optimal tuned conditions for both the TVA and the TMD may be found in a number of sources, including Den Hartog [1] and Harris [2]. If ω_{exc} is uncertain or varies and if significant attenuation is desired, the TVA and the TMD both have limitations and more sophisticated vibration control solutions are required, including active, active–passive, and adaptive–passive vibration control solutions. Bernhard et al. [3] provide definitions for those different classifications. The active-mass driver described by Spencer et al. [4] is an example of an active device, while the active vibration isolator described by Miller et al. [5] is an example of an active–passive approach to vibration control.

The adaptive tuned vibration absorber (ATVA) is an adaptive–passive vibration control device similar to a TVA but with adaptive elements that can be used to change the ATVA tuned condition. Most commonly, adaptive stiffness elements are used to vary the device natural frequency such that an ATVA may be tuned to track uncertain or time-varying excitation frequencies. At the same time, the ATVA is generally simpler than completely active approaches

due to the less stringent actuator demands. For an ATVA, actuator bandwidth is related to the rate of change of ω_{exc}.

Two challenges exist for adaptive–passive solutions. The first is the incorporation of adaptability into the physical design, for which one method is discussed in this paper. The second challenge is the controller design to direct the on-line adaptation, which will be dealt with in later work.

1.1. ATVA mechanical design

ATVA designs may be broken down into two main groups; designs that use variable geometries and designs that use active materials. The variable leaf-spring design of Walsh and Lamancusa [6] and the variable-length coil-spring design of Franchek et al. [7] and Buhr et al. [8] are examples of variable-geometry ATVA designs. The device described by Seto and Tominari [9] is similar to an ATVA, but is used for broadband vibration control, much like a TMD. While not used for vibration control, the variable-volume Helmholtz resonator described by de Bedout et al. [10] is very similar to an ATVA in design and implementation.

Sun et al. [11] cited "reliability and maintainability concerns" of ATVA designs with moving parts and mechanisms and suggested the use of active materials as alternatives. An early example of this approach was discussed by Forward [12], who shunted piezoelectric strain transducers with resistor–inductor circuits to increase the damping in an underlying structure. Hagood and von Flotow [13] later provided descriptions of the modelling and application of passively shunted piezoelectric devices in vibration control. Von Flotow et al. [14] further suggested the use of variable electrical circuits to extend operation to situations with varying excitation frequencies, an active materials realization of an ATVA.

Experimental results of on-line tuning of active materials were provided by Hollkamp and Starchville [15] for variably shunted piezoelectric patches mounted on a vibrating beam. Hollkamp and Starchville's device was an adaptive TMD which was tuned to attenuate broadband vibration. Davis et al. [16] suggested the use of a piezoceramic inertial actuator (PIA) as an adaptive TVA and reported the use capacitive shunts to vary the PIA natural frequency from 243 to 257 Hz. Davis and Lesieutre [17] later applied a commercially available PIA to a primary system and used external circuits to vary the shunt capacitance during a frequency sweep with substantial improvements in the steady state vibration attenuation. The magnetostrictive material Terfenol-D was used by Flatau et al. [18] to develop an ATVA incorporating a pre-stressed Terfenol-D rod that achieved a natural frequency variation from 1400 to over 2000 Hz through application of DC magnetic fields.

Shape memory alloys (SMA) have also been used in a few adaptive–passive vibration control applications. The most well-known characteristic of SMA is the shape memory effect, the ability of the material to recover from apparently plastic deformations through the application of heat due to a transformation between a low temperature phase martensite and a high temperature phase austenite, the so-called martensitic transformation. In addition to the shape memory effect, SMA material properties such as elastic modulus can change significantly through the transformation. In the SMA Nitinol, the material elastic modulus will vary by a factor as high as three during the transformation. A potential limitation of the martensitic transformation is a significant temperature hysteresis. The transformation from martensite to austenite occurs over a

higher temperature range than the reverse transformation, with differences of as much as 10–20°C between the two regions. While this temperature hysteresis may be a positive characteristic in some SMA applications, it is generally undesirable in vibration control and may destabilize automatic controllers.

In addition to martensite and austenite, a third phase, the R-phase may be present in Nitinol depending on the heat treatment of the material, as described by Uchil et al. [19] and Lei and Wu [20]. While the shape memory effect is significantly smaller for the R-phase transformation than for the martensitic transformation, significant variation in the material elastic modulus is still achieved, as reported by Lei and Wu [20]. However, in contrast to the martensitic transformation, the R-phase transformation occurs with little or no temperature hysteresis. Lei and Wu [20] demonstrate a temperature hysteresis that appears to be on the order of 2°C or less in contrast to a hysteresis of greater than 20°C in an identical specimen with a different heat treatment. When testing a comparable sample of material, Pelosin and Riviere [21] reported that "no thermal hysteresis has been detected for the R phase". The low hysteresis of the R-phase transformation is an attractive characteristic for use of NiTi for vibration control applications requiring a variation in the material elastic modulus.

The shape memory effect has been used in a number of different approaches to vibration control. SMA has been used to add active structural tendons to a structure as described by Shahin et al. [22] and for offset SMA wire actuators as described by Baz et al. [23]. An adaptive–passive approach was taken by Nagaya et al. [24], who describe the use of SMA actuated bearings on a rotating shaft. In their work, Regelbrugge and Hurlbut [25] described two uses of SMA for adaptive–passive vibration isolation mounts. One technique was to use high-temperature SMA with a mechanical hysteresis loop to optimize the stiffness and damping in passive leaf springs. As a second approach, the authors suggested the use of variable radius SMA leaf springs.

Williams et al. [26] used the variable modulus of SMA to develop a discretely tuned SMA ATVA. Identical pairs of small circular NiTi beams were embedded in an end-mass and mounted in a fixture such that the effect was of a cantilevered beam with a tip-mass, referred to as a mass-ended cantilevered beam. Resistive heating of individual SMA beam pairs was used to vary each pair's temperature between "cold" and "hot" states. Using three pairs of SMA beams, four discrete tuned conditions were possible. A plot of the primary system's vibration response with and without the SMA ATVA is shown in Fig. 3. The points on the plot represent the steady state performance of the system to tonal excitation at each excitation frequency.

While the SMA ATVA described by Williams et al. [26] was successfully applied to a situations with discrete known excitation frequencies, if the excitation frequencies are not known or if they drift, the discretely tuned SMA ATVA may be an inappropriate solution due to the limited number of tuned conditions available for a given design and the diminished performance which occurs at intermediate frequencies. As shown in Fig. 3, performance diminishes during the frequency variation between 84 and 88 Hz. Similar behavior was reported by Davis and Lesieutre [17], who used discrete changes in shunt capacitances to realize different tuned conditions of their ATVA.

Increasing the number of discrete tuned conditions available for a given ATVA will result in improved performance at intermediate frequencies. For Davis and Lesieutre [17], additional external shunt relays and capacitors would be required. For Williams et al. [26], additional pairs of SMA beams would be required, which would soon result in a cluttered and unwieldy

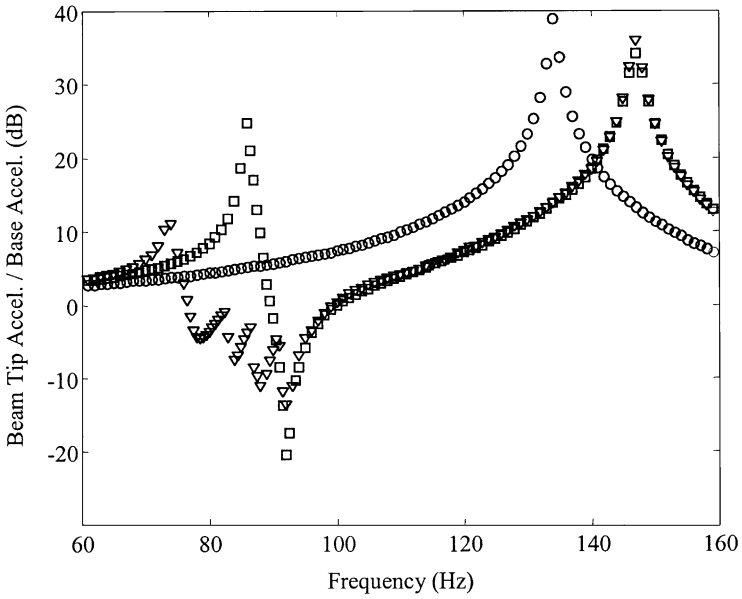

Fig. 3. Primary system performance plots: ○, no TVA; □, passive TVA; ▽, discretely tuned SMA ATVA.

mechanical design. In both cases, performance improvements would require significantly increased system complexity.

An alternative is to replace discrete tuning with continuous tuning. Davis and Lesieutre [17] alluded to this approach but indicated that such an approach may not be practical due to the small ranges of available variable capacitors and the "added complexity and resistance" of programmable capacitors.

Temperature modulation may be used to achieve continuous tuning of the SMA ATVA described by Williams et al. [26]. Heating the SMA elements to intermediate temperatures within the transformation temperature range should result in corresponding partial shift of the device natural frequency. This new approach requires a modified experimental apparatus to provide continuously variable power to the SMA elements. In addition, a new control algorithm will be required, along with an appropriate error signal to indicate the quality of the tuned condition. The development of control algorithms for adaptive–passive devices is discussed in the next section.

1.2. Control of adaptive–passive devices

Because adaptive–passive designs are direct descendents of passive devices, there is a strong tendency to take the conditions for optimality of a passive device and develop these into tuning laws. For example, in a typical adaptive tuned mass damper (ATMD), it is best to have the ATMD natural frequency close to the resonant frequency of the primary system. That open-loop control logic was used by Seto and Tominari [9] and Walsh and Lamancusa [6]. However, to achieve robust performance in the presence of uncertainty requires closed-loop control. Basic work in this area was performed by Hollkamp and Starchville [15] and de Bedout et al. [10], who

both implemented gradient searches to minimize the system response. Davis and Lesieutre [17] also used closed-loop control by comparing a frequency estimate against a pre-determined plot of shunt capacitance versus frequency that had been developed through prior analysis of experimental responses.

A control algorithm based on the theory of the undamped TVA was proposed by Franchek et al. [7] and Buhr et al. [8]. For an undamped TVA, when $\omega_{abs} = \omega_{exc}$, there is a 90° phase lag between the acceleration of the TVA and the acceleration of the primary mass. Working on that principle, they designed a feedback controller that used the relative phase signal to determine the ATVA tuning direction. The magnitude of the control signal was proportional to the magnitude of the vibration and thus the adaptive–passive control problem was posed as a classical feedback control problem with a signed error signal. While this approach was successfully demonstrated, no analysis of the system stability was presented.

1.3. The continuously tuned SMA ATVA

The attractiveness of the adaptive passive approach to vibration control is the potential for using relatively simple systems to realize significant steady state vibration attenuation with an approach that is robust to changes in excitation frequency or system variations. The results presented by Davis and Lesieutre [17] and Williams et al. [26] suggest that robust performance might be realized through the use of continuous tuning. Robust performance will require closed-loop algorithms which in turn, require system models that reliably predict dynamic device behavior.

The rest of this paper describes the study of a continuously tuned SMA ATVA for use in control of harmonic vibration. The work is split into three main areas. First, experimental testing of an SMA ATVA was performed to determine system behavior and generate dynamic response data. The data was then used to produce an analytical model for predicting the system's dynamic behavior. Based on that model, the relative phase between the vibration of the SMA ATVA and the primary system was examined as a measure of the quality of the system's tuned condition. In the final step of the work, the previous results were experimentally validated. The results of this research indicate the potential of the SMA ATVA for use in adaptive–passive vibration control and serve as a foundation for future work on the design of ATVA controllers.

2. SMA ATVA construction and testing

2.1. SMA ATVA design and construction

As described previously, during transformations between austenite and either martensite or R-phase material, the elastic modulus of the SMA Nitinol varies significantly. To take advantage of the variable elastic modulus, a mass-ended cantilevered beam was chosen for the prototype SMA ATVA. The natural frequency of such a system is given by Blevins [27] as

$$\omega_{abs} = \sqrt{\frac{3EI}{L^3(M_{end} + 0.24m_{beam})}}, \tag{1}$$

where E is the beam material elastic modulus, I is the beam cross-sectional inertia, L is the beam length, m_{beam} is the beam mass, and M_{end} is the end mass. The terms in Eq. (1) may be separated into an effective mass and stiffness, $m^* = (M_{end} + 0.24m_{beam})$ and $k^* = 3EI/L^3$, respectively. An SMA beam may thus be treated as an adaptive stiffness element. If beam elements composed of inert materials such as steel are used in parallel with the SMA beam elements, the EI term in Eq. (1) is the sum of the EI terms of the individual beam elements. Eq. (1) is then rewritten as

$$\omega_{abs} = \sqrt{\frac{3(E_{inert}I_{inert} + E_{SMA}I_{SMA})}{L^3(M_{end} + 0.24m_{beam})}}. \tag{2}$$

Use of inert materials in parallel with SMA reduces the amount of stiffness variation for a given ATVA design. This may be desirable, particularly in applications where the required range of tuning is small. Also, at temperatures below the austenitic start temperature (A_s), the material has a relatively low yield stress. While a certain amount of plastic yielding is non-damaging in SMA, the yielding will produce a mechanical hysteresis resulting in a non-linear behavior with increased damping. As such, steel beam elements were used in parallel with the SMA elements, both to confine the tuning range and to reduce damping and nonlinearities.

Following these design guidelines, a prototype SMA ATVA was constructed using 4 SMA and 2 steel circular beams clamped in an end mass. The ATVA dimensions are listed in Table 1. To provide on-line adaptation, the SMA beam elements were electrically wired in series and connected to a DC power supply.

2.2. Demonstration of R-phase transformation

As noted previously, the standard martensitic transformation may have significant temperature hysteresis that could degrade or destabilize the closed-loop system. For that reason, it was important to utilize an SMA material exhibiting the R-phase transformation. To test the SMA material for the R-phase transformation, an SMA beam cut from the same stock used in the SMA ATVA was wired to the output of a DC power supply. The power supply provided a constant 0.5 A current through the beam. A step current of 4.5 A was then superimposed over the original 0.5 A for 300 s. After 300 s the current was reduced to 0.5 A of current for an additional 300 s. The beam resistance, R_{SMA} was calculated based on voltage and current measurements. A plot of R_{SMA} as a function of beam temperature T_{SMA} is shown in Fig. 4. The noisier trace is the plot of R_{SMA} versus T_{SMA} during the second half of the test, where the signal-to-noise ratio of the voltage measurements was significantly diminished due to the smaller current levels. A classical "s-curve"

Table 1
SMA AVTA dimensions

r_{steel}	1.06 mm
r_{SMA}	1.22 mm
L	6 cm
M_{end}	132 g
m_{beam}	7.24 g

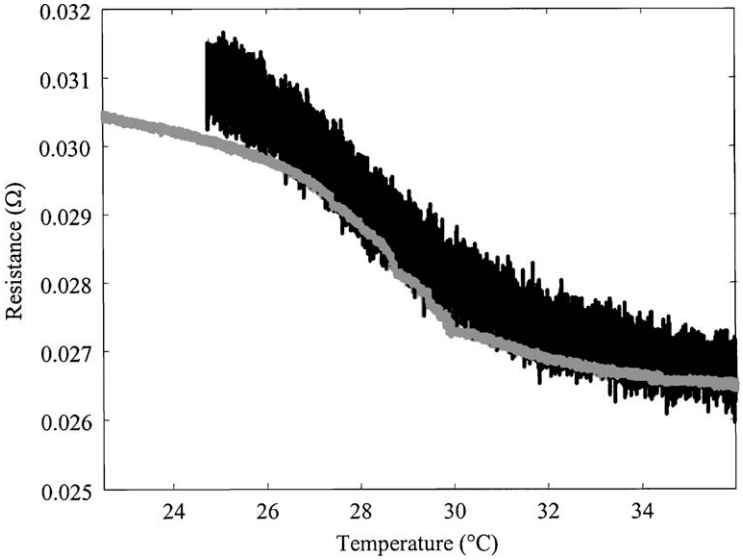

Fig. 4. SMA resistance versus temperature: ——, heating; ——, cooling.

occurs where there is a significant drop in R_{SMA}, especially from approximately 27°C to 30°C. The drop in R_{SMA} is indicative of the transformation from the R-phase austenite in the SMA. A similar transition is shown in the work by Lei and Wu [20].

There is an apparent anomaly in Fig. 4. The transformation from austenite to R-phase occurs at a higher temperature (approximately 0.5°C across the transformation) than the reverse transformation. This is believed to be an artifact of the method used for heating the SMA beam. Some difference between the indicated temperature at the beam surface and the actual temperature of the cross-section will occur during cooling but not during heat generation. These effects were not investigated in this work. The transformations of interest take place across a very narrow temperature region.

2.3. Dynamic response of the SMA ATVA and primary system

To determine the dynamic response of the SMA ATVA as a function of temperature, the device was mounted on an electromagnetic shaker and driven with stepped-sine inputs from 20 to 50 Hz while the shaker armature and SMA ATVA end-mass accelerations were recorded. SMA beam temperatures were measured using a thermocouple attached to one of the beams. The beam temperatures were held constant for the duration of each of 18 tests for SMA beam temperatures between 60°C and 16°C. To enable testing at the lower end of the transformation temperature region, a mobile air conditioning unit was used to cool the ambient air in the area of the experimental set-up to approximately 15°C. The resulting frequency response functions are shown in Fig. 5. For the sake of clarity, only eight of the 18 responses are shown. The natural frequency of the SMA ATVA varies with the temperature of the SMA elements. Thus, temperature modulation may be used to control the tuned condition of the SMA ATVA.

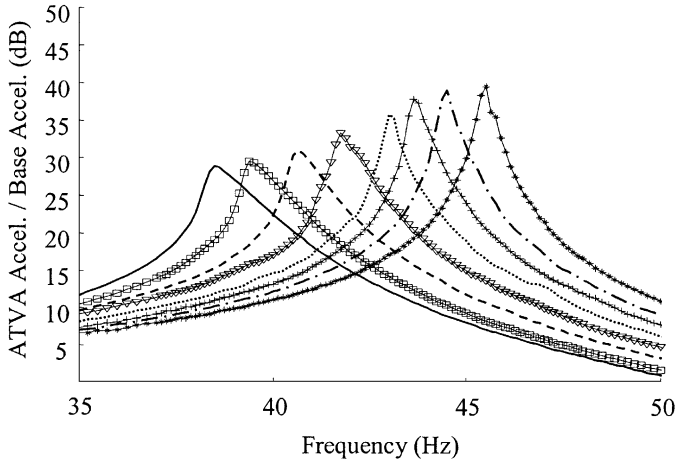

Fig. 5. ATVA frequency responses: —, 16°C; -□-, 22°C; - - -, 23°C; -▽-, 24°C; ....., 25°C; —|—, 30°C; — · —, 33°C; —∗—, 42°C.

Table 2
Primary system dimensions

b_b	38 mm
h_b	9.5 mm
L	152 mm
M_{end}	550 g
m_{beam}	1000 g

To determine the impact of the SMA ATVA on the vibration of a primary system, the SMA ATVA system was attached to a primary system composed of a larger mass-ended cantilevered beam. The new beam was steel. The primary system dimensions are listed in Table 2. The coupled system was clamped to the shaker and excited with a series of 0.2 g stepped-sine tests from 34 to 110 Hz. Frequency responses between the shaker input acceleration and the primary system's end-mass acceleration were recorded for 15 constant SMA beam temperatures between 16°C and 42°C. Four of the frequency responses are shown in Fig. 6 along with the frequency response of the primary system without the SMA ATVA. It is apparent that application of the SMA ATVA can be used to achieve vibration attenuation of more than 5 dB at 38.5 Hz to more than 30 dB at 46.5 Hz. The variation of attenuation is attributed to the greater apparent damping of SMA material at lower temperatures, which will be discussed further in a later section.

3. SMA ATVA system modelling

Based on the results of the previous section, it is apparent that for harmonic excitation at a specific frequency that there is a corresponding SMA beam element temperature that will provide

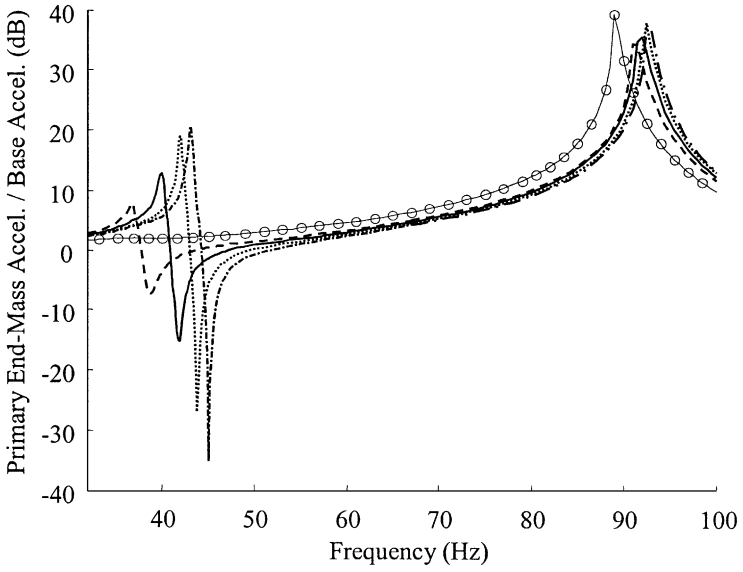

Fig. 6. Primary system frequency responses: –○–, no ATVA; ---, ATVA 16°C; —, ATVA 21°C; ...., ATVA 24°C; –·–, ATVA 42°C.

the best attenuation of the primary system vibration. If a reliable map of beam temperature versus frequency is available, open-loop control of the SMA ATVA could be accomplished by simply measuring the instantaneous excitation frequency and using a feedback controller to achieve the prescribed beam temperature. However, the relationship between SMA beam surface temperature and the tuned condition of the SMA ATVA may depend on additional factors such as humidity, ambient air temperature and flow. As such, a control algorithm acting only to control the temperature of the SMA elements may not be robust. A more direct method of controlling the system is required based on some metric of the quality of the tuned condition. This section describes a proposed metric and the development of a dynamic model to predict its transient behavior.

3.1. Control goal and required system models

Ideally, a metric describing the tuned condition of the SMA ATVA will be a signal with both magnitude and sign. For a fixed excitation frequency ω_{exc}, the tuned condition for an undamped absorber occurs at $\cos(\phi_{rel}) = 0$, where ϕ_{rel} is the relative phase between the absorber vibration and the primary system vibration. Thus $\phi_{rel} = \phi_{ATVA} - \phi_P = -90^\circ$, where ϕ_P is the phase of the primary mass acceleration and ϕ_{ATVA} is the phase of the ATVA acceleration. For an ATVA tuned to a frequency above ω_{exc}, the two masses respond in-phase with $\phi_{rel} = 0^\circ$ such that $\cos(\phi_{rel}) = 1$. Conversely, an ATVA tuned to a frequency less than ω_{exc} results in the two masses vibrating out of phase with $\phi_{rel} = -180^\circ$ such that $\cos(\phi_{rel}) = -1$. Thus, for an undamped TVA, $\cos(\phi_{rel}) = 0$ can be used to determine the quality of a tuned condition. If damping is present in the absorber, $\cos(\phi_{rel}) = 0$ is no longer an exact indicator of the optimum tuned condition. Either, some other

indicator must be established or operation at the sub-optimal condition of $\cos(\phi_{rel}) = 0$ must be tolerated.

For a damped absorber, the transfer function between the base acceleration input and the primary system acceleration output is

$$\frac{s^2 x_P(s)}{s^2 x_b(s)} = \frac{(m_a s^2 + c_a s + k_a)(c_P s + k_P)}{[m_P s^2 + (c_P + c_a)s + (k_P + k_a)](m_a s^2 + c_a s + k_a) - (c_a s + k_a)^2}, \tag{3}$$

where $s^2 x_b(s)$ and $s^2 x_P(s)$ are the Laplace transforms of $\ddot{x}_b(t)$ and $\ddot{x}_P(t)$. m_a, m_P, c_a, c_P, k_a, and k_P are the absorber and primary system mass, damping, and stiffness, respectively. For a given problem, m_P, c_P, k_P, and m_a are fixed and are not available as design variables. To determine the optimal SMA ATVA stiffness k_a^* for each c_a, the following optimization problem must be solved:

$$\min_{k_a^*} \left| \frac{(k_a^* - m_a\omega_{exc}^2 + \mathrm{j}\omega_{exc}^2 \cdot c_a)(\mathrm{j}\omega_{exc}^2 c_P + k_P)}{[(k_P + k_a^*) - m_P\omega_{exc}^2 + \mathrm{j}(c_P + c_a)](k_a^* - m_a\omega_{exc}^2 + \mathrm{j}\omega_{exc}^2 \cdot c_a) - (\mathrm{j}\omega_{exc}^2 c_a + k_a^*)^2} \right| \tag{4}$$

subject to $0 < k_a^* \leqslant k_{max}$.

An optimization routine was used to determine the k_a^* to minimize the objective function of Eq. (4) for each of a set of c_a values given fixed m_P, c_P, k_P, and m_a. Values for m_P, c_P, k_P, and m_a are listed in Table 3. The optimum relative phase ϕ_{rel}^* at that tuned condition is given by

$$\phi_{rel}^* = \tan^{-1}\left(\frac{-c_a m_a \omega_{exc}^3}{(k_a^*)^2 - k_a^* m_a \omega_{exc}^2 + (c_a)^2 \omega_{exc}^2} \right). \tag{5}$$

The frequency responses of the primary system with the $\{k_a, c_a\}$ pairs were calculated and are shown in Figs. 7 and 8. For each case, $\cos(\phi_{rel}^*)$ was calculated. A plot of $\cos(\phi_{rel}^*)$ against the absorber damping ratio ζ_a is shown in Fig. 9. As ζ_a increases, $\cos(\phi_{rel}^*)$ move away from $\cos(\phi_{rel}) = 0$. Thus, $\cos(\phi_{rel}) = 0$ is not an exact indicator of the optimum tuned condition.

To calculate the performance loss anticipated by operating at the condition $\cos(\phi_{rel}) = 0$, the k_a values to achieve $\cos(\phi_{rel}) = 0$ at ω_{exc} were also determined for each c_a value. The primary system response magnitude was then calculated at the excitation frequency for each $\{k_a, c_a\}$ combination. Plots of achievable vibration attenuation are shown in Fig. 10 for the cases of both the absorber tuned to achieve the true optimal $\cos(\phi_{rel}^*)$ and for absorber tuned to achieve $\cos(\phi_{rel}) = 0$. The loss in vibration attenuation is shown in Fig. 11. Operation at $\cos(\phi_{rel}) = 0$ results in a maximum loss of approximately 0.9 dB in vibration attenuation. That peak performance loss occurs at $\zeta_a \approx 3.5\%$. However, when operating at the optimal $\cos(\phi_{rel}^*)$ for high damping, the vibration attenuation has dropped to less than 5 dB. To achieve better performance, ζ_a must be reduced. As

Table 3
Primary system and TVA parameters for $\cos(\phi_{rel})$ study

m_P	0.55 kg
k_P	217,000 N/m
c_P	15 N-s/m
m_a	0.132 kg
ω_{exc}	42.5 Hz

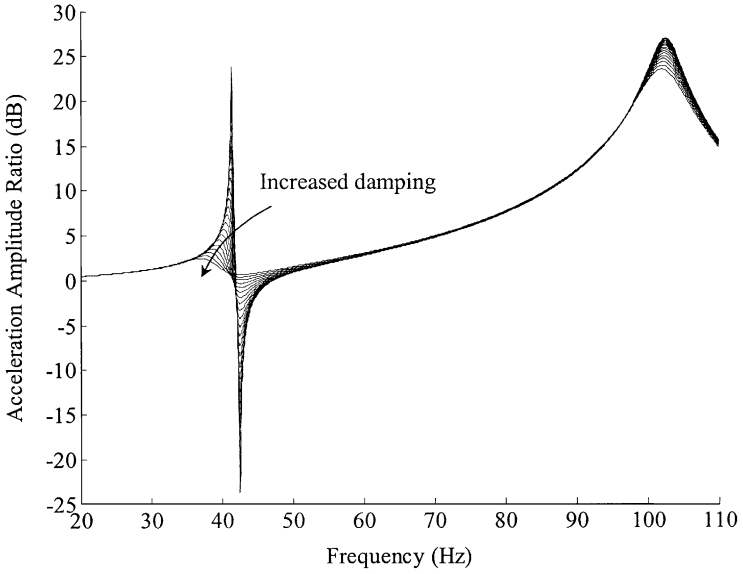

Fig. 7. Primary system magnitudes with different TVA.

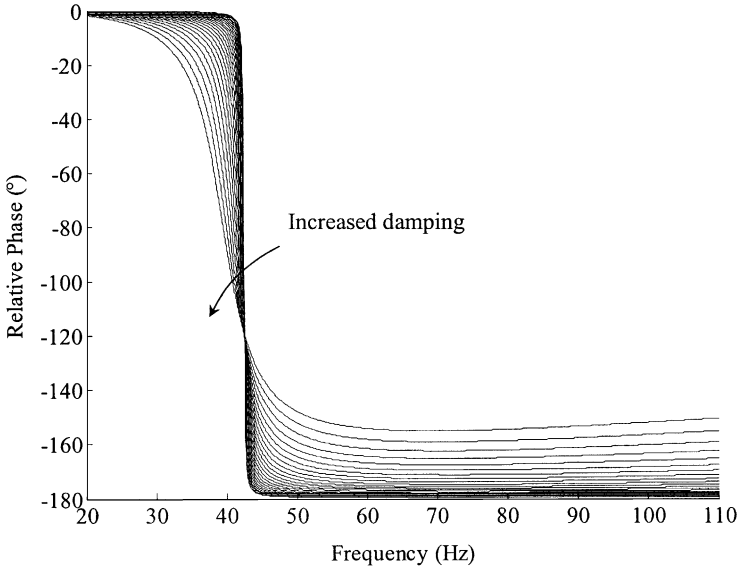

Fig. 8. Primary system phases with different TVA.

ζ_a is reduced, the difference between $\cos(\phi_{rel}) = 0$ and $\cos(\phi^*_{rel})$ is smaller. Based on this result, $\cos(\phi_{rel}) = 0$ is an acceptable measure for many implementations.

For those applications where the optimal value of $\cos(\phi_{rel})$ for a given excitation condition will be required, exact analytical determination of the optimal $\cos(\phi_{rel})$ may be difficult. This is due to the difficulties inherent in determining the damping of both the SMA ATVA and the primary system. To find the optimal tuning condition either offline or preliminary investigations could be

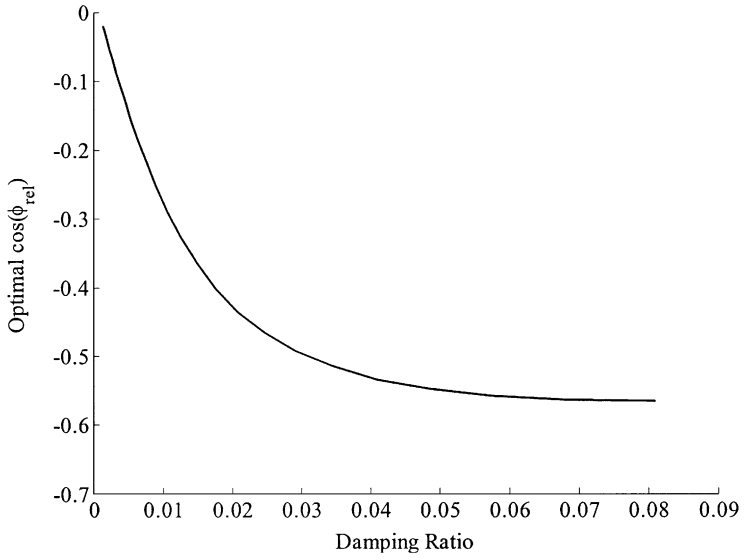

Fig. 9. Optimum $\cos(\phi_{rel})$ for different damped absorbers.

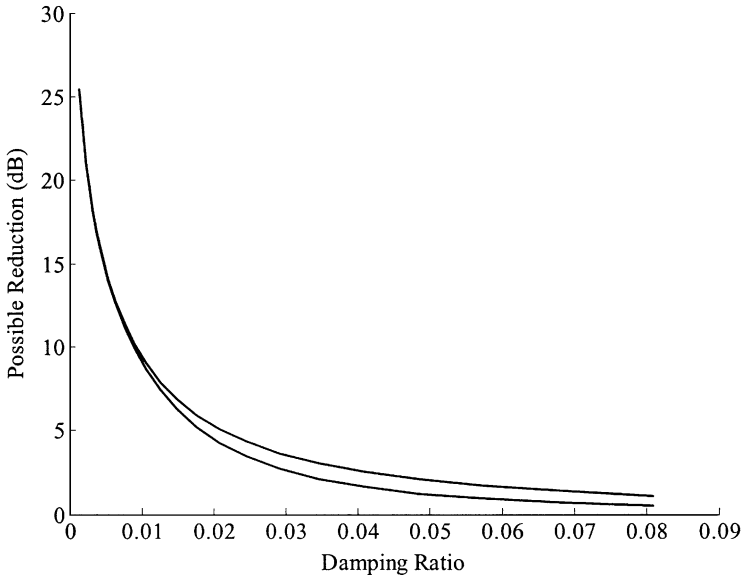

Fig. 10. Possible vibration reduction using absorbers tuned to the different $\cos(\phi_{rel})$ values: —, $\cos(\phi_{rel}) = 0$; - -, $\cos(\phi_{rel}) =$ optimal.

used to experimentally determine the optimum $\cos(\phi_{rel})$ values for various operating conditions. Alternatively, it may be possible to use a gradient search or other similar search algorithms to determine the optimum $\cos(\phi_{rel})$.

The coupled system SMA ATVA and primary system described in Section 2.3 was used to demonstrate the variation of $\cos(\phi_{rel})$ during tuning of the SMA ATVA. The SMA beam elements

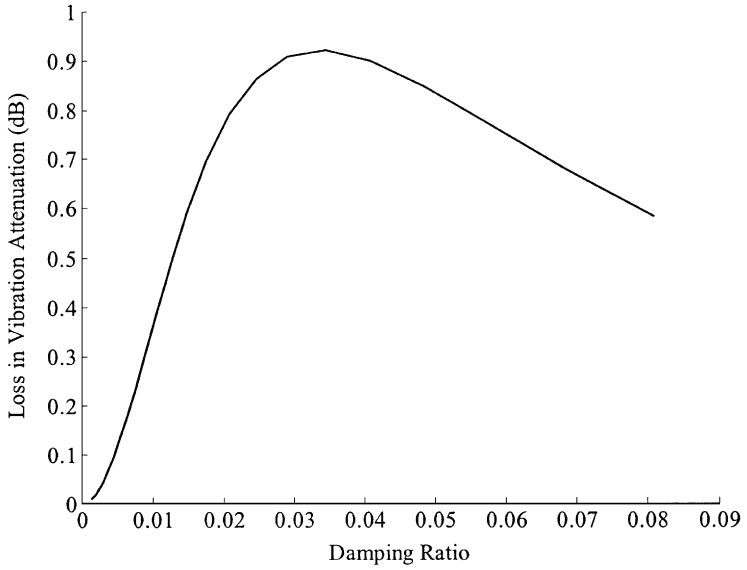

Fig. 11. Loss in vibration reduction by using $\cos(\phi_{rel}) = 0$ for a control goal.

were initially at a temperature of approximately 19.5°C. The shaker was used to provide a 0.2 g, 42.7 Hz acceleration to the SMA ATVA system for 720 s. After 30 s, an 8.7 A current was applied to the SMA beams for 360 s. The current was then turned off and data was recorded for an additional 330 s. The measured current $i(t)$ and SMA element temperature $x_T(t)$ are shown in Fig. 12. The corresponding primary mass acceleration $\ddot{x}_P(t)$ is shown in Fig. 13. After the test, $\cos(\phi_{rel})$ was evaluated from $\ddot{x}_P(t)$ and the ATVA acceleration $\ddot{x}_a(t)$ using the digital cross-correlation

$$\cos(\phi_{rel}) = \frac{\ddot{x}_P^{\mathrm{T}} \cdot \ddot{x}_a}{|\ddot{x}_P| \cdot |\ddot{x}_a|}, \tag{6}$$

where $\ddot{x}_P$ and $\ddot{x}_a$ were moving vectors of 768 points of $\ddot{x}_P(t)$ and $\ddot{x}_a(t)$.

The resulting estimate of $\cos(\phi_{rel}(t))$ is plotted over the record of $\ddot{x}_P(t)$ and is shown in Fig. 13. $\cos(\phi_{rel})$ starts near -1 as the SMA ATVA is initially cold and has a natural frequency significantly below the excitation frequency at 42.7 Hz. As the SMA beams are heated, $\cos(\phi_{rel})$ increases, and passes through zero at approximately the same time as $\ddot{x}_P(t)$ reaches a minimum magnitude. $\cos(\phi_{rel})$ continues to increase toward $+1$ as $x_T(t)$ and the magnitude of $\ddot{x}_P(t)$ also increase. When the current is removed from the SMA beams, $x_T(t)$ and $\cos(\phi_{rel})$ decrease and $\cos(\phi_{rel})$ again goes through zero at approximately the same time as $\ddot{x}_P(t)$ reaches a minimum magnitude.

The approximate coincidence of $\cos(\phi_{rel}) = 0$ and the minimum $|\ddot{x}_P(t)|$ verifies that $\cos(\phi_{rel}) = 0$ is a reasonable control goal for this absorber.

3.2. SMA ATVA modelling

The objective of this work is the development of a dynamic model for an SMA ATVA applied to a primary system. The plant model is shown in Fig. 14, where the input $u(t)$, is the squared

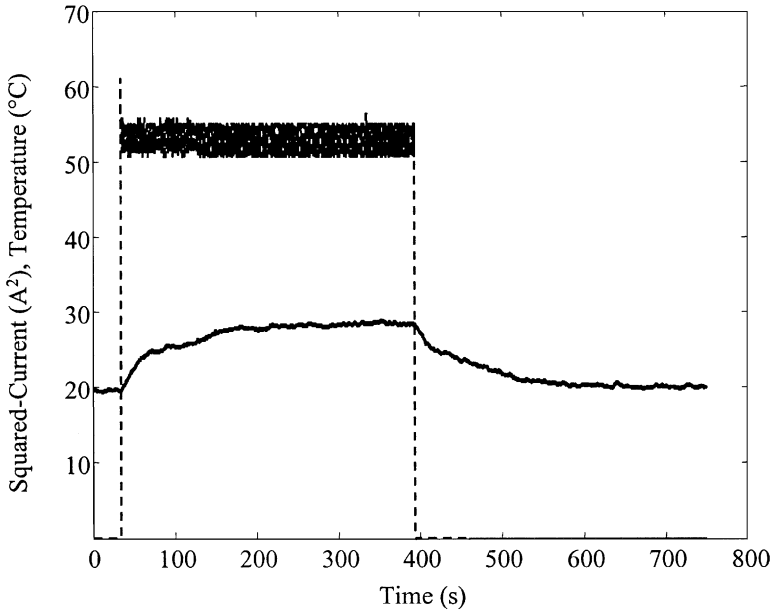

Fig. 12. SMA element temperature responses to step input in i^2: - - -, squared current (A^2); —, temperature (°C).

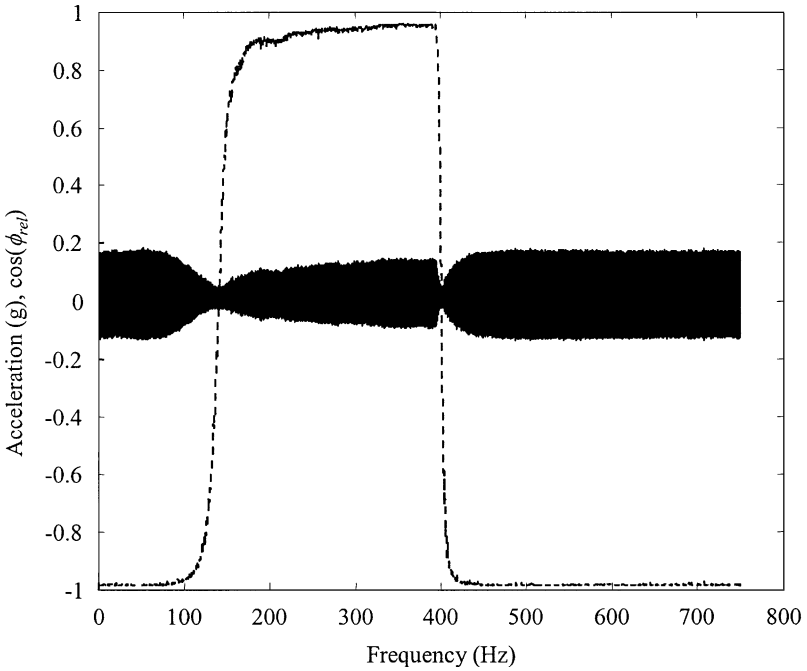

Fig. 13. Primary mass response to 49 A^2 step input: —, acceleration; - -, $\cos(\phi_{rel})$.

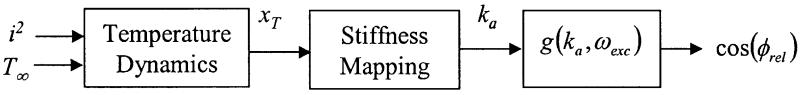

Fig. 14. Open-loop system.

electrical current from the DC power supply, i^2, x_T is the SMA beam temperature, k_a is the effective absorber stiffness, and $\cos(\phi_{rel})$ is the plant output. Three basic mappings must be considered: the mapping from u to x_T , the mapping from x_T to k_a, and the mapping from k_a to $\cos(\phi_{rel})$ for a given excitation frequency ω_{exc}.

Joule-effect heating was used to heat the SMA beams by passing an electrical current through the beams and assuming power dissipation equal to $(i^2 \cdot R)$, where R is the series resistance of the SMA beams. Cooling was assumed to occur through free convection. As has been discussed, the SMA resistance will vary significantly across the phase transformations. For example, the resistance of the material used in the SMA ATVA decreased by approximately 15% during the transformation from R-phase to austenite. A constant-coefficient first order model was used to simplify the SMA ATVA temperature dynamics. It is unlikely that this simplified model will contribute to significant errors, although if the results indicate that higher fidelity models are required, the dependence of the SMA resistance on temperature may be addressed in a subsequent work. The temperature dynamics are

$$\dot{x}_T = -\frac{1}{\tau} x_T + \frac{k_T}{\tau} u + \frac{1}{\tau} T_\infty, \tag{7}$$

where the controller output is $u(t) = i^2$; τ and k_T were determined by fitting first order models of the form of Eq. (7) to experimental results of the SMA elements heating behavior with step inputs of squared-current from the DC power supply. Current and temperature data during the test were recorded for squared-current step inputs of 75 and 100 A^2 as plotted in Fig. 15. Based on those tests, the values for τ and k_T are approximately 45 and 0.155, respectively. A simulation of Eq. (7) was written in Simulink. The simulation results are shown in Fig. 15 superimposed over the experimental data. Based on the comparison between the experimental and simulated responses in Fig. 15, the temperature dynamics of Eq. (7) appear to be a good approximation of the temperature dynamics of the SMA ATVA for purposes of controller design.

The temperature results also demonstrate two additional characteristics of the SMA ATVA. First, to maintain a tuned condition will require a non-zero current input to the SMA elements. Second, the time constant associated with the temperature dynamics is significant. There will be an upper limit on the rate at which the SMA ATVA will be able to track an excitation source with a varying frequency.

3.3. Stiffness mapping

Least-squares estimations of k_a and c_a were performed by fitting the experimental frequency response data shown in Fig. 5 to the lumped parameter model for a simple mass–spring–damper system,

$$\frac{s^2 x_a(s)}{s^2 x_b(s)} = \frac{c_a s + k_a}{m_a s^2 + c_a s + k_a}. \tag{8}$$

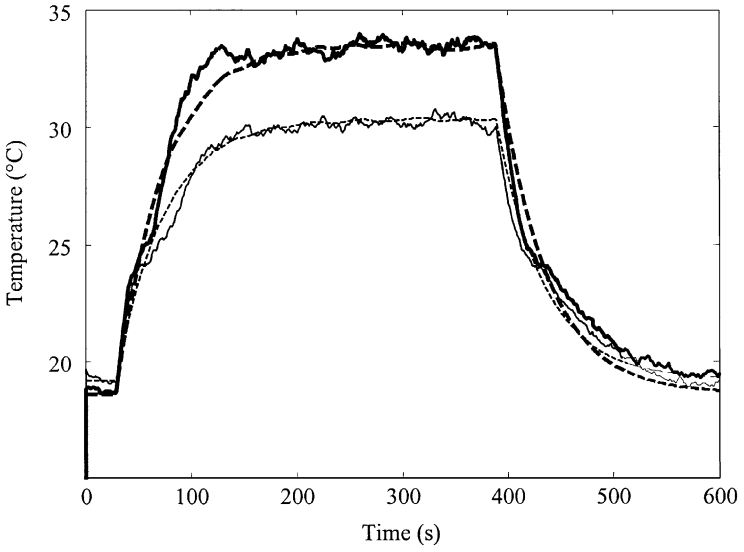

Fig. 15. SMA wire temperature response to i^2 step inputs: —, 75 A^2 actual; - - -, 75 A^2 simulated; ——, 100 A^2 actual; — –, 100 A^2 simulated.

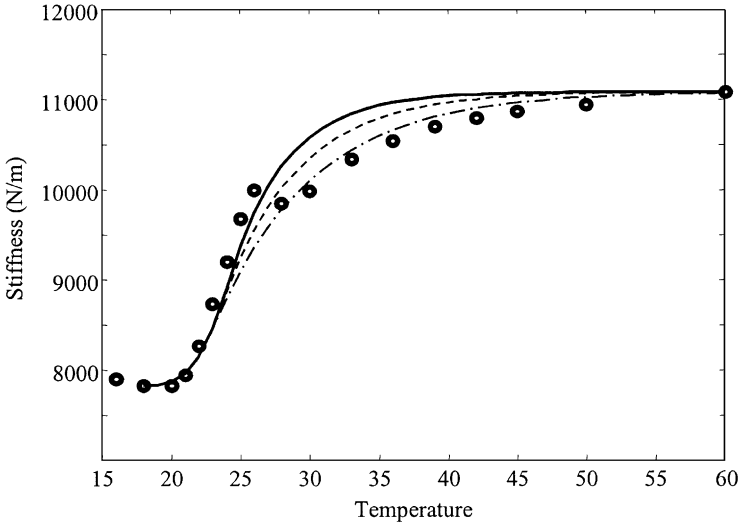

Fig. 16. SMA ATVA stiffness versus temperature: O, experimental; —, $T_{trans} = 23$; - - -, $T_{trans} = 23.5$; – · –; $T_{trans} = 24$.

The SMA ATVA mass m_a was chosen according to the approximation $m_a = M_{end} + 0.24m_b$. $s^2x_b(s)$ and $s^2x_b(s)$ are the Laplace transforms of $\ddot{x}_b(t)$ and $\ddot{x}_a(t)$. Based on the estimation m_a, k_a, and c_a, the SMA ATVA damping ratio ζ_a was calculated as a function of temperature. Plots of k_a and ζ_a are shown in Figs. 16 and 17, respectively. As mentioned previously, the damping of the SMA elements is greater at lower temperatures. This is also apparent in the frequency response plots of Figs. 5 and 6. However, based on those figures, the damping is still sufficiently light to

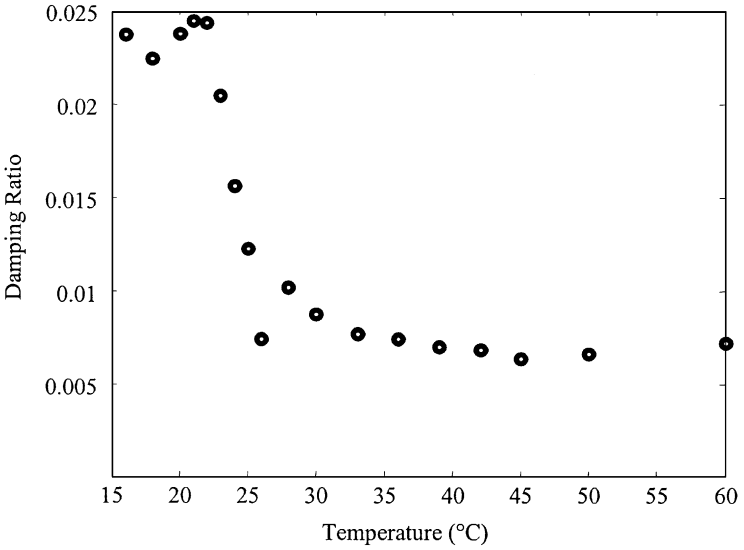

Fig. 17. SMA ATVA damping ratio versus temperature.

provide substantial attenuation of the primary mass vibration across the operating frequency range.

A basic model was developed to estimate k_a versus temperature behavior by fitting a cubic polynomial to the experimental data below 23.5°C and a first order function of temperature for data above 23.5°C. The curve-fit is

$$k_a(T) = \begin{cases} \alpha(x_T - T_{kmin})^3, & T < T_{trans}, \\ k_{max} - (k_{max} - k_{trans})\mathrm{e}^{-3\alpha(x_T - T_{kmin})^2(x_T - T_{trans})/(k_{max} - k_{trans})}, & T > T_{trans}, \end{cases} \tag{9}$$

where α is the gain for the cubic form, T_{kmin} is the temperature of the minimum stiffness (18°C), and k_{max} is the maximum estimated stiffness from the experimental data of Fig. 16 (11,081 N/m). k_{trans} is the stiffness evaluated at the temperature T_{trans}, the temperature where the model transitions from the cubic form to the first order response form. The two functions have identical derivatives at T_{trans}. By changing T_{trans} and maintaining the smooth transitions between the two forms, different stiffness approximations can be developed. Three curves for $k_a(T)$ are shown superimposed over the experimental data in Fig. 16 for T_{trans} values of 23°C, 23.5°C, and 24°C. The three models were chosen to show the dependence of the model parameters on the fit.

Other stiffness approximations besides those of Eq. (9) could have been used, as well. For example, Liang and Rogers [28] used a (1 − cos) function to model the martensitic transformation in SMA. The current model was chosen to accurately reflect the different variations of stiffness with temperature across the temperature range.

There is a slight decrease in stiffness with temperature when the SMA is heated from 16°C to 18°C. However, that stiffness variation is relatively small in comparison to the variation at temperatures above 18°C. As such, assuming that the stiffness is a strictly increasing function with temperature should not result in any significant errors in the system model.

3.4. $\cos(\phi_{rel})$ versus stiffness mapping

At steady state, the relative phase between the vibration absorber and the primary mass is given by the formula

$$\phi_{rel} = \arctan\left(\frac{-c_a m_a \omega_{exc}^3}{k_a^2 - k_a m_a \omega_{exca}^2 + c_a^2 \omega_{exc}^2}\right), \tag{10}$$

where m_a and c_a are the SMA ATVA mass and damping, respectively. If the argument of the arctan function is defined as

$$f(k_a, \omega_{exc}) = \frac{-c_a m_a \omega_{exc}^3}{k_a^2 - k_a m_a \omega_{exca}^2 + c_a^2 \omega_{exc}^2}, \tag{11}$$

then

$$\cos^2(\phi_{rel}) = \frac{1}{1 + f^2(k_a, \omega_{exc})},$$

and

$$\cos(\phi_{rel}) = \begin{cases} \sqrt{\dfrac{1}{1 + f^2(k_a, \omega_{exc})}}, & f(k_a, \omega_{exc}) < 0, \\ -\sqrt{\dfrac{1}{1 + f^2(k_a, \omega_{exc})}}, & f(k_a, \omega_{exc}) > 0. \end{cases} \tag{12}$$

A key assumption in the development of Eq. (12) is that the steady state relationship between the absorber stiffness and $\cos(\phi_{rel})$ is valid for situations where the absorber stiffness is a time-varying quantity. This assumption is true if the stiffness can be considered a slowly varying parameter compared to the frequency of the vibration of the system. The time constants for the temperature dynamics were found to be on the order of tens of seconds. By comparison, the approximate frequency range for excitation of the current SMA ATVA is from 35 to 50 Hz. The separation between the bandwidth of the stiffness variation and the excitation frequency is sufficiently large to allow the assumption of the steady state relationship for $\cos(\phi_{rel}(k_a, \omega_{exc}))$.

3.5. Complete SMA ATVA plant description

When the individual SMA ATVA sub-system models are combined, the complete mathematical description of the system is

$$\dot{x}_T = -\frac{1}{\tau} x_T + \frac{k_T}{\tau} u + \frac{1}{\tau} T_\infty, \tag{13}$$

$$\cos(\phi_{rel}) = \begin{cases} \sqrt{\dfrac{1}{1 + f^2(k_a, \omega_{exc})}}, & f(k_a, \omega_{exc}) < 0, \\ -\sqrt{\dfrac{1}{1 + f^2(k_a, \omega_{exc})}}, & f(k_a, \omega_{exc}) > 0, \end{cases}$$

where $k_a(x_T)$ and $f(k_a, \omega_{exc})$ are given by Eqs. (9) and (10), respectively. Assuming a constant excitation frequency ω_{exc}, there exists an equilibrium temperature x_{eq} such that $k_{eq} = k_a(x_{eq})$ and

$\cos(\phi_{rel}(x_{eq})) = 0$. x_{eq} is the SMA beam temperature that corresponds to the target tuned condition for the given ω_{exc}. That condition is achieved when the SMA beam temperature x_T matches x_{eq}. If the perturbation of x_T about x_{eq} is defined as $\tilde{x} = (x_T - x_{eq})$, then the mathematical description of the perturbed system is given by

$$\dot{\tilde{x}} = -\frac{1}{\tau}\tilde{x} + \frac{k_T}{\tau}u - \frac{1}{\tau}(x_{eq} - T_\infty), \tag{14}$$

$$y = \cos(\phi_{rel}(\tilde{x})) = \begin{cases} \sqrt{\dfrac{1}{1+f^2(k_a(\tilde{x}),\omega_{exc})}}, & f(k_a(\tilde{x}),\omega_{exc}) < 0, \\ -\sqrt{\dfrac{1}{1+f^2(k_a(\tilde{x}),\omega_{exc})}}, & f(k_a(\tilde{x}),\omega_{exc}) > 0, \end{cases}$$

where

$$f(k_a(\tilde{x}),\omega_{exc}) = \frac{-c_a m_a \omega_{exc}^3}{k_a^2(\tilde{x}) - k_a(\tilde{x}) m_a \omega_{exc}^2 + c_a^2 \omega_{exc}^2}.$$

The general expression $k_a(\tilde{x})$ is determined by replacing x_T with $(\tilde{x} + x_{eq})$ in Eq. (9).

For the majority of the operating temperature range the output $y = \cos(\phi_{rel}(\tilde{x}))$ is always in the first and third quadrants and is a strictly increasing function where

$$\cos(\phi_{rel}(\tilde{x})) = \begin{cases} \cos(\phi_{rel})|_{min}, & \{x_T < T_{min}\}, \\ \cos(\phi_{rel})|_{max}, & \{x_T > T_{max}\}. \end{cases} \tag{15}$$

$\cos(\phi_{rel})|_{min}$ and $\cos(\phi_{rel})|_{max}$ correspond to $\cos(\phi_{rel}(\tilde{x}))$ when the SMA beams are at temperatures outside of the transformation temperature region for the material. Typical behavior of $\cos(\phi_{rel}(\tilde{x}))$ is shown in Fig. 18. The only exception to the strictly increasing characteristic of Eq. (15) would be for operation at an equilibrium temperature of 18°C or less, where for a very narrow region, increases in temperature may result in slight decreases in stiffness, as indicated previously.

3.6. SMA ATVA system model verification

To validate the model of Eq. (13), a simulation of an SMA ATVA was created using the software Simulink and compared to experimental data. The model was then exercised with the parameters listed in Table 4. To generate the experimental data, the SMA ATVA and primary system were mounted on an electromagnetic shaker and excited with a 0.2 g signal at 42.7 Hz. The SMA beam temperature was then measured as a step current was applied to the SMA elements, held constant for a period of time, and then removed. During the test, the acceleration of the primary mass and SMA ATVA end-mass were recorded and used to generate $\cos(\phi_{rel})$ as described by Eq. (6). The simulated and experimental data for $x_T(t)$ are plotted in Fig. 15. The corresponding $\cos(\phi_{rel}(t))$ for 75 and 100 A^2 inputs are plotted in Figs. 19 and 20.

For the 75 A^2 input for each of the different T_{trans} values the simulated $\cos(\phi_{rel}(t))$ lags the experimental data during the heating regime and leads it during cooling regimes. The best fit is achieved by using the lowest transition temperature, $T_{trans} = 23°C$. For the 100 A^2 input, the simulated $\cos(\phi_{rel}(t))$ still lags the experimental data during the heating phase, but by significantly

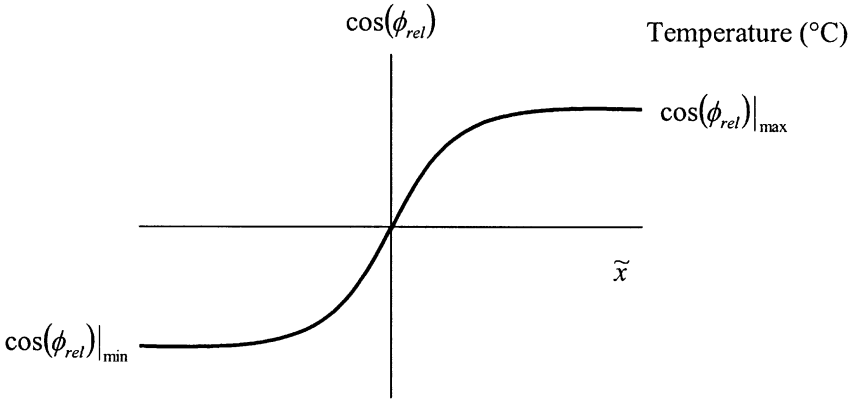

Fig. 18. Sketch of $\cos(\phi_{rel}(\tilde{x}))$.

Table 4
SMA AVTA system simulation parameters

T_{kmin}	18°C
T_{trans}	23°C, 23.5°C, 24°C
k_{min}	7824 N/m
k_{max}	11081 N/m
c_a	1 N-s/m
k_T	0.155°C/amp^2
τ	45 s
ω_{exc}	42.7 Hz
T_∞	19.4°C (100 A^2 test)
	18.6°C (75 A^2 test)

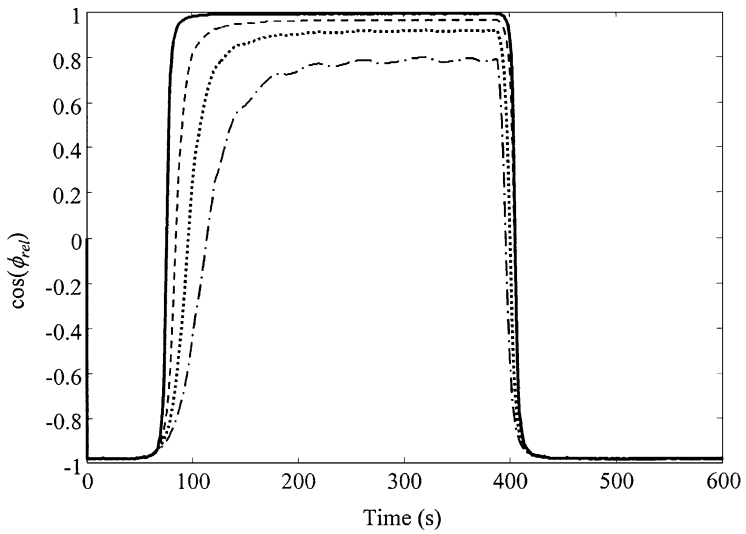

Fig. 19. $\cos(\phi_{rel}(t))$ for 75 A^2 input: —, experimental; - - -, $T_{trans} = 23$; ⋯, $T_{trans} = 23.5$; – · –, $T_{trans} = 24$.

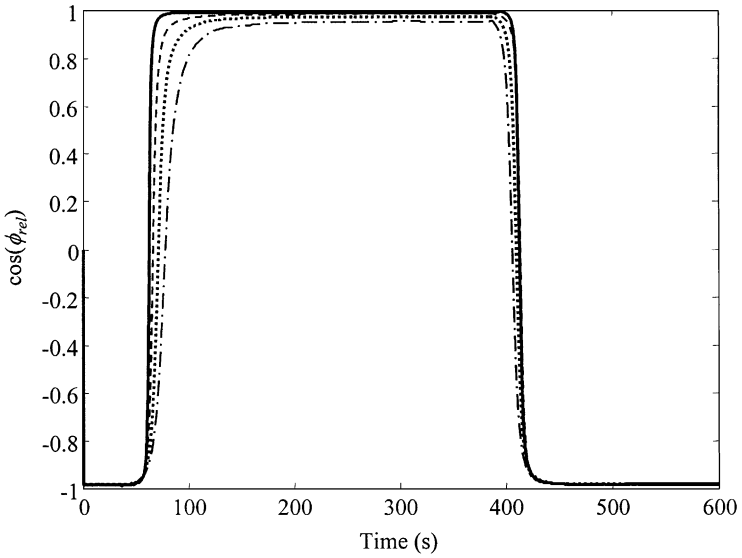

Fig. 20. $\cos(\phi_{rel}(t))$ for 100 A^2 input: —, experimental; - - -, $T_{trans} = 23$; ⋯, $T_{trans} = 23.5$; $-\cdot-$, $T_{trans} = 24$.

less than for the 75 A^2 input. The best fit match is achieved using $T_{trans} = 23^\circ C$. During cooling, the simulated and experimental $\cos(\phi_{rel}(t))$ traces are essentially simultaneous for $T_{trans} = 23^\circ C$.

The fit between the simulated and experimental results is believed to be sufficiently close to justify the use of the system model in the design of an ATVA controller. If a better fit was desired, the experiments could be improved by performing them in a system with a more tightly regulated temperature than is available in the current open laboratory space.

4. Conclusions

This paper has presented the continuously tuned SMA ATVA as a novel adaptive–passive vibration control device. The design and construction of an SMA ATVA utilizing the R-phase transformation were described. Testing showed that the SMA ATVA natural frequency could be varied by approximately 15%, with a corresponding reduction in the steady state vibration of a primary system of up to 40 dB. Models for the transient temperature of the SMA beam elements and the static map between the SMA beam element temperature and the corresponding ATVA stiffness were also developed. Those models were used as the foundation for a model that predicts the transient behavior of the SMA ATVA when applied to a primary system. The results have demonstrated the potential for the SMA ATVA as a device for use in vibration control. Other geometries could also be investigated to consider the constraints of application-specific needs such as rattle-space or mounting details. However, this work has demonstrated the feasibility of designing a continuously tuned SMA ATVA and the resulting model is available for future work on feedback controller design.

References

[1] J.P. Den Hartog, *Mechanical Vibrations*, McGraw-Hill, New York, 1956.
[2] C.M. Harris, *Shock and Vibration Handbook*, 4th Edition, McGraw-Hill, New York, 1996.
[3] R.J. Bernhard, H.R. Hall, J.D. Jones, Adaptive–passive noise control, *Proceedings of the Inter-Noise*, 1992, pp. 427–430.
[4] B.F. Spencer, S.J. Dyke, H.S. Deoskar, Benchmark problems in structural control, Part I: active mass driver system, *Earthquake Engineering and Structural Dynamics* 27 (11) (1998) 1127–1139.
[5] L.R. Miller, M. Ahmadian, C.M. Nobles, D.A. Swanson, Modeling and performance of an experimental active vibration isolator, *Journal of Vibration and Acoustics* 117 (3a) (1995) 272–278.
[6] P.L. Walsh, J.S. Lamancusa, A variable stiffness vibration absorber for minimization of transient vibrations, *Journal of Sound and Vibration* 158 (2) (1992) 195–211.
[7] M.A. Franchek, M.W. Ryan, R.J. Bernhard, Adaptive passive vibration control, *Journal of Sound and Vibration* 189 (5) (1995) 565–585.
[8] C. Buhr, M.A. Franchek, R.J. Bernhard, Non-collocated adaptive–passive vibration control, *Journal of Sound and Vibration* 206 (3) (1997) 371–398.
[9] K. Seto, N. Tominari, Effect of a variable stiffness-type dynamic damper on machine tools with long overhung ram, *Bulletin of the JSME* 19 (137) (1976) 1270–1277.
[10] J.M. de Bedout, M.A. Franchek, R.J. Bernhard, L. Mongeau, Adaptive–passive noise control with self-tuning Helmholtz reasonators, *Journal of Sound and Vibration* 202 (1) (1997) 109–123.
[11] J.Q. Sun, M.R. Jolly, M.A. Norris, Passive, adaptive, and active tuned vibration absorbers—a survey, *Journal of Mechanical Design* 117B (1995) 234–242.
[12] R.L. Forward, Electronic damping of vibrations in optical structures, *Applied Optics* 18 (5) (1979) 690–697.
[13] N.W. Hagood, A.H. Von Flotow, Damping of structural vibrations with piezoelectric materials and passive electrical networks, *Journal of Sound and Vibration* 146 (2) (1991) 243–268.
[14] A.H. Von Flotow, A. Beard, D. Bailey, Adaptive tuned vibration absorbers: tuning laws, tracking agility, sizing, and physical implementations, *Proceedings—National Conference on Noise Control Engineering*, *Progress in Noise Control for Industry*, 1994, pp. 437–454.
[15] J.J. Hollkamp, T.F. Starchville, A self-tuning piezoelectric vibration absorber, *Journal of Intelligent Material Systems and Structures* 5 (4) (1994) 559–566.
[16] C.L. Davis, G.A. Lesieutre, J. Dosch, A tunable electrically shunted piezoceramic vibration absorber, *Proceedings of SPIE*, Vol. 3045, 1995, pp. 51–59.
[17] C.L. Davis, G.A. Lesieutre, An actively tuned solid-state vibration absorber using capacitive shunting of piezoelectric stiffness, *Journal of Sound and Vibration* 232 (3) (2000) 601–617.
[18] A.B. Flatau, M.J. Dapino, F.T. Calkins, High bandwidth tenability in a smart vibration absorber, *Proceedings of SPIE*, Vol. 3327, 1998, pp. 463–473.
[19] J. Uchil, K.P. Mohanchandra, K.K. Mahesh, K. Ganesh Kumar, Thermal and electrical characterization of R-phase dependence on heat-treat temperature in Nitinol, *Physica B* 253 (1998) 83–89.
[20] C.Y. Lei, Ming H. Wu, Thermoelectrical properties of NiTi-base shape memory alloys, *Smart Structures and Materials, American Society of Mechanical Engineers Aerospace Division* AD 24 (1991) 73–77.
[21] V. Pelosin, A. Riviere, Effect of thermal cycling on the R-phase and martensitic transformations in a Ti-rich NiTi alloy, *Metallurgical and Materials Transactions A* 29A (1998) 1175–1180.
[22] A.R. Shahin, P.H. Meckl, J.D. Jones, Modeling of SMA tendons for active control of structures, *Journal of Intelligent Materials Systems and Structures* 8 (1) (1997) 51–70.
[23] A. Baz, K. Imam, J. McCoy, Active vibration control of flexible beam using shape memory actuators, *Journal of Sound and Vibration* 140 (3) (1990) 437–456.
[24] K. Nagaya, S. Takeda, Y. Tsukui, T. Kumaido, Active control method for passing through critical speeds of rotating shafts by changing stiffnesses of the supports with use of memory metals, *Journal of Sound and Vibration* 113 (2) (1997) 307–315.
[25] M.E. Regelbrugge, B.J. Hurlbut, Design of shape-memory alloy vibration isolators, *Proceedings of the Fourth International Conference on Adaptive Structures*, 1994, pp. 559–572.

[26] K.A. Williams, G.T.-C. Chiu, R.J. Bernhard, Passive–adaptive vibration absorbers using shape memory alloys, *Proceedings of the SPIE*, Vol. 3668, 1999, pp. 630–641.
[27] R.D. Blevins, *Formula for Natural Frequency and Mode Shape*, Van Nostrand Reinhold, New York, 1979.
[28] C. Liang, C.A. Rogers, One-dimensional thermomechanical constitutive relations for shape memory materials, *Journal of Intelligent Material Systems and Structures* 8 (4) (1997) 285–302.